

# Families of fundamental and multipole solitons in a cubic-quintic nonlinear lattice in fractional dimension

Liangwei Zeng,<sup>1,2</sup> Dumitru Mihalache,<sup>3</sup> Boris A. Malomed,<sup>4,5</sup>  
Xiaowei Lu,<sup>1,2</sup> Yi Cai,<sup>1,2</sup> Qifan Zhu,<sup>1,2</sup> and Jingzhen Li<sup>1,2,\*</sup>

<sup>1</sup>*College of Physics and Optoelectronic Engineering, Shenzhen University, Shenzhen 518060, China*

<sup>2</sup>*Shenzhen Key Laboratory of Micro-Nano Photonic Information Technology,*

*College of Physics and Optoelectronics Engineering, Shenzhen University, Shenzhen 518060, China*

<sup>3</sup>*Horia Hulubei National Institute of Physics and Nuclear Engineering, Magurele, Bucharest, RO-077125, Romania*

<sup>4</sup>*Department of Physical Electronics, School of Electrical Engineering,*

*Faculty of Engineering, and the Center for Light-Matter Interaction,  
Tel Aviv University, P.O.B. 39040, Ramat Aviv, Tel Aviv, Israel*

<sup>5</sup>*Instituto de Alta Investigación, Universidad de Tarapacá, Casilla 7D, Arica, Chile*

We construct families of fundamental, dipole, and tripole solitons in the fractional Schrödinger equation (FSE) incorporating self-focusing cubic and defocusing quintic terms modulated by factors  $\cos^2 x$  and  $\sin^2 x$ , respectively. While the fundamental solitons are similar to those in the model with the uniform nonlinearity, the multipole complexes exist only in the presence of the nonlinear lattice. The shapes and stability of all the solitons strongly depend on the Lévy index (LI) that determines the FSE fractionality. Stability areas are identified in the plane of LI and propagation constant by means of numerical methods, and some results are explained with the help of an analytical approximation. The stability areas are broadest for the fundamental solitons and narrowest for the tripoles.

**key words:** Multipole solitons; Cubic-quintic nonlinear lattice; Fractional Schrödinger equation

## I. INTRODUCTION

It is commonly known that stable bright and dark solitons exist in one-dimensional uniform self-focusing and self-defocusing nonlinear media, respectively [1, 2]. However, the situation may be totally different in higher dimensions, where bright solitons are destabilized by the collapse [3–10]. One of solutions to this problem is offered by the use of spatially inhomogeneous settings [11–16]. First, linear periodic potentials [17–22], which are induced by optical lattices in Bose-Einstein condensates (BECs), or photonic lattices in optical waveguides, help to stabilize various types of self-trapped modes, including fundamental [23], dipole [24], and vortex [12, 25–27] solitons. Another option is the use of periodic spatial modulation of the local nonlinearity strength, alias nonlinear lattices [28]. Many types of solitons are maintained in nonlinear lattices [29–31], *viz.*, fundamental ones, as well as dipole, tripole, and vortex solitons. In addition, combinations of linear and nonlinear lattices can be used to stabilize various species of solitons [32–34]. Inhomogeneous self-defocusing nonlinearity [35–37] is another setting in which many species of stable self-trapped modes have been predicted, such as multipole [35, 36] and vortex [38–41] solitons, vortex clusters [42, 43], skyrmions [44], soliton gyroscopes [45], and flat-top solitons [46, 47]. Inhomogeneous nonlinearities can be implemented by means of creation of a spatially nonuniform distribution of dopants in photorefractive optical media [48]. In BEC, similar setups can be created too, using the Feshbach res-

onance controlled by spatially nonuniform external fields [49–51].

In this work, we aim to address the possibility of using nonlinear lattices as an ingredient of the fractional Schrödinger equation (FSE), which was introduced by Laskin two decades ago in the context of quantum mechanics [52–55]. The main parameter that defines the fractionality of the FSE is the Lévy index (LI),  $\alpha$ , see Eq. (1) below. The experimental implementation of the FSE in condensed-matter [56, 57] and optical [58] setups, where nonlinearity is a natural feature, has drawn interest to the possibility of existence of solitons in fractional dimensions [59–62]. In particular, “accessible solitons” [63, 64] and self-trapped states of vectorial [65], gap [66], nonlocal [67], vortical [68], and multi-peak types [69] have been predicted in FSE models, as well as soliton clusters [70, 71], symmetry breaking of solitons [72, 73], coupled solitons [74] and dissipative solitons in a fractional complex-Ginzburg-Landau model [75]. In the case of the ubiquitous cubic (Kerr) self-focusing, the solitons are unstable at  $\alpha \leq 1$ , as the combination of such values with the Kerr nonlinearity gives rise to the collapse.

The objective of this work is to identify domains of existence and stability of fundamental and multipole (dipole and tripole) solitons in FSE with a nonlinear lattice combining the cubic self-focusing and quintic defocusing (vortices produced by the FSE including the uniform cubic-quintic (CQ) nonlinearity were recently addressed in Ref. [68]). While fundamental solitons produced by this model are not strongly different from their counterparts in the one with the uniform nonlinearity, it opens a way to create stable multipoles, *i.e.*, complexes of solitons with opposite signs placed at adjacent sites of the lattice.

\* [lijz@szu.edu.cn](mailto:lijz@szu.edu.cn)

The rest of the paper is organized as follows. In Sec. II we present the model and the method used for the linear-stability analysis. Then, in Sec. III, we summarize extensive numerical results that make it possible to outline the stability domains for the fundamental solitons and multipoles, *viz.*, dipole and tripole bound states. These results, based on the computation of eigenvalues for small perturbations, are corroborated by direct simulations of perturbed propagation dynamics of the solitons. The paper is concluded in Sec. IV.

## II. THE MODEL

The FSE modeling the propagation of a light beam with field amplitude  $E$  under the action of the fractional diffraction in the medium with the CQ spatially modulated nonlinearity is written in the normalized form:

$$i \frac{\partial E}{\partial z} = \frac{1}{2} \left( -\frac{\partial^2}{\partial x^2} \right)^{\alpha/2} E - g(x) |E|^2 E + \xi(x) |E|^4 E, \quad (1)$$

where  $z$  is the propagation distance, while the fractional diffraction operator with LI  $\alpha$  is defined by the integral expression [52, 76],

$$\begin{aligned} \left( -\frac{\partial^2}{\partial x^2} \right)^{\alpha/2} E &= \frac{1}{2\pi} \int_{-\infty}^{+\infty} |p|^\alpha dp \\ &\times \int_{-\infty}^{+\infty} d\xi \exp[ip(x - \xi)] E(\xi), \end{aligned} \quad (2)$$

the limit of  $\alpha = 2$  corresponding to the usual second derivative. In the case of the cubic-only self-focusing nonlinearity, LI is limited by values  $\alpha > 1$ , as the collapse occurs at  $\alpha \leq 1$ , as mentioned above. However, the inclusion of the quintic term with the defocusing sign suppresses the collapse and makes it possible to consider values  $\alpha < 1$  as well [68], although the solutions tend to be unstable in the latter case, see Fig. 2(b) below. Note that, in the case of constant nonlinearity coefficients  $g$  and  $\xi$ , Eq. (1) admits continuous-wave (CW) solutions with an arbitrary real wavenumber  $k$  and arbitrary amplitude  $E_0$ :

$$\begin{aligned} E_{\text{CW}} &= E_0 \exp(ib_{\text{CW}}z + ikx), \\ b_{\text{CW}} &= -\frac{1}{2}|k|^\alpha + gE_0^2 - \xi E_0^4. \end{aligned} \quad (3)$$

The nonlinear lattice is introduced, replacing the constant coefficients by the spatially-modulated ones:

$$g(x) = \cos^2 x, \quad \xi(x) = \sin^2 x. \quad (4)$$

Here, the lattice period and amplitudes are fixed, severally, to be  $\pi$  and 1, by means of rescaling. Stationary solutions with real propagation constant  $b$  are sought for as  $E(x, z) = U(x)\exp(ibz)$  (cf. the CW solution (3)),

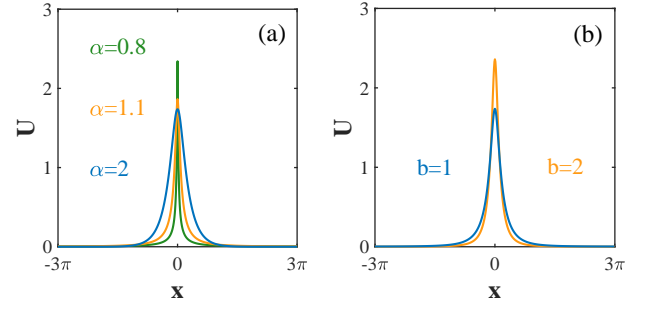


FIG. 1. Profiles of fundamental solitons: (a) with different values of LI (Lévy index)  $\alpha$ , for propagation constant  $b = 1$ ; (b) with different values of  $b$ , for  $\alpha = 1.5$ . Note that  $\alpha = 2$  corresponds to the usual local (non-fractional) Schrödinger equation.

where the stationary field,  $U(x)$ , satisfies the following equation:

$$-bU = \frac{1}{2} \left( -\frac{\partial^2}{\partial x^2} \right)^{\alpha/2} U - (\cos^2 x) |U|^2 U + (\sin^2 x) |U|^4 U. \quad (5)$$

Soliton solutions to Eq. (2) are characterized by their integral power,

$$P = \int_{-\infty}^{+\infty} |U(x)|^2 dx. \quad (6)$$

Equation (5) is solved below by dint of the modified squared-operator method [77].

The linear-stability analysis will be performed for a perturbed solution taken as

$$E = [U(x) + p(x)\exp(\lambda z) + q^*(x)\exp(\lambda^* z)]\exp(ibz), \quad (7)$$

where  $p(x)$  and  $q^*(x)$  represent the eigenmode of small perturbations corresponding to eigenvalue  $\lambda$  (the instability growth rate). The eigenmodes are solutions of the linearized equations produced by the substitution of ansatz (7) in Eq. (1):

$$\begin{aligned} i\lambda p &= +\frac{1}{2} \left( -\frac{\partial^2}{\partial x^2} \right)^{\alpha/2} p + bp - (\cos^2 x) U^2(2p + q) \\ &\quad + (\sin^2 x) U^4(3p + 2q), \end{aligned} \quad (8)$$

$$\begin{aligned} i\lambda q &= -\frac{1}{2} \left( -\frac{\partial^2}{\partial x^2} \right)^{\alpha/2} q - bq + (\cos^2 x) U^2(2q + p) \\ &\quad - (\sin^2 x) U^4(3q + 2p). \end{aligned}$$

The solitons are stable if  $\text{Re}(\lambda) = 0$  for all eigenvalues. The so predicted (in)stability will be verified through direct numerical simulations of the full evolution equation (1), performed by means of the split-step Fourier method.

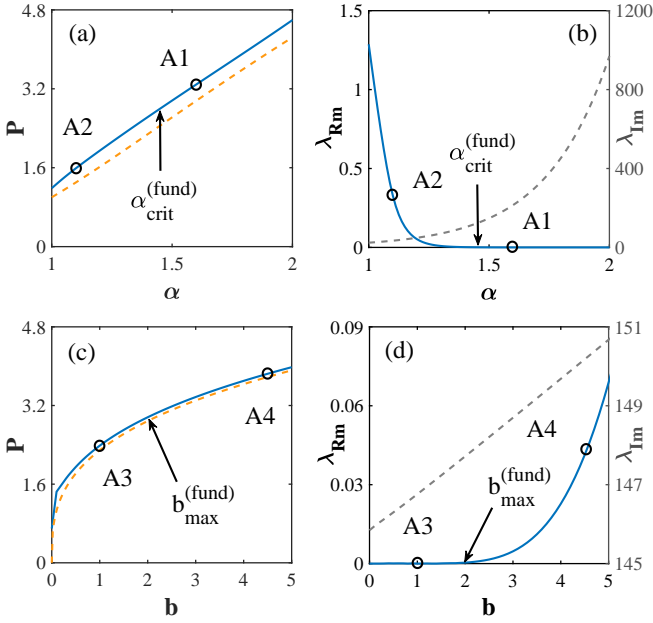


FIG. 2. Soliton's power  $P$  (a) and the maximum real part of eigenvalues (instability growth rate)  $\lambda_{Rm}$  (b) versus  $\alpha$  for fundamental solitons at  $b = 2$ . In panel (b), the vertical arrow indicates the boundary of the stability region, with very weak instability to the left of it. Power  $P$  (c) and  $\lambda_{Rm}$  (d) versus  $b$  for fundamental solitons at  $\alpha = 1.5$ . The arrow in panel (d) indicates the respective boundary of the stability region. Panels (a) and (c) include the best-fit approximation (red dashed lines) provided by Eq. (9), with  $\text{const} = 9$  and  $12$ , respectively. Panels (b) and (d) include the imaginary part,  $\lambda_{Im}$  (gray dashed lines), corresponding to  $\lambda_{Rm}$ . Simulations of perturbed evolution of the fundamental solitons marked by labels A1–A4 are displayed in Figs. 3(a–d), respectively.

### III. NUMERICAL RESULTS

In this Section, we report numerical findings for solitons in the FSE with the CQ lattice, including their profiles, stability domains, and perturbed propagation. The Section is divided in two parts, which address, separately, fundamental and multipole (dipole and tripole) solitons.

#### A. Fundamental solitons

Typical profiles of fundamental stationary solitons are presented in Fig. 1. Naturally, the maximum of the local intensity is located at  $x = 0$ , where the self-focusing and defocusing coefficients in Eq. (5) attain, respectively, a maximum and minimum (zero). Accordingly, the soliton is stabilized by being placed at the bottom of an effective nonlinear potential well induced by the spatially-modulated CQ nonlinearity. In fact, Fig. 1 demonstrates that the fundamental solitons are completely confined to a spatial interval  $|x| < 3\pi/4$ , hence Eq. (5) suggests that the shape of the solitons is chiefly determined by

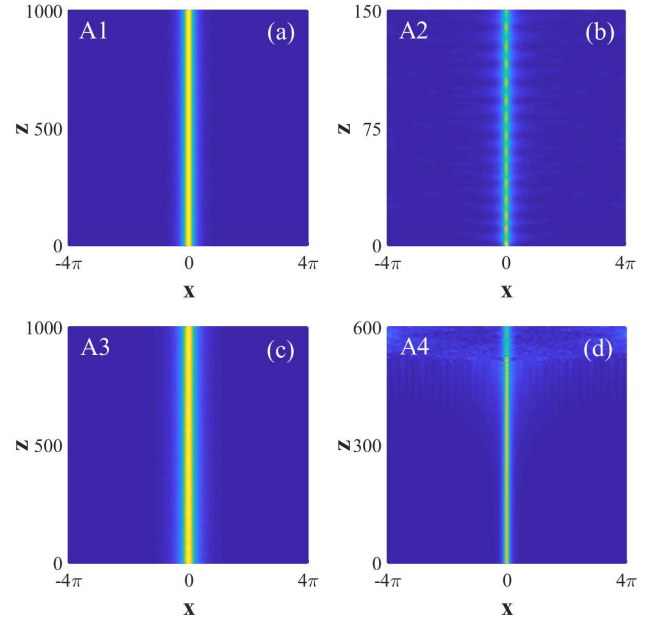


FIG. 3. The propagation of perturbed fundamental solitons: (a) a stable soliton with  $\alpha = 1.6$ ,  $b = 2$ ; (b) an unstable one with  $\alpha = 1.1$ ,  $b = 2$ ; (c) a stable soliton with  $\alpha = 1.5$ ,  $b = 1$ ; (d) an unstable one with  $\alpha = 1.5$ ,  $b = 4.5$ .

the cubic term. Then, taking, for an approximate estimate, a constant value of the respective coefficient,  $g$  (see Eq. (1)), Eq. (5) predicts a scaling relation between the propagation constant, amplitude, and width ( $W$ ):  $b \sim W^{-\alpha} \sim A^2$ , which determines the approximate scaling of the integral power,

$$P \sim A^2 W \sim (\text{const} \cdot b)^{1-1/\alpha}. \quad (9)$$

As LI  $\alpha$  increases, the amplitude  $A$  of the fundamental soliton decreases, while its width increases, as seen in Fig. 1(a). In this figure, the amplitudes are  $A(\alpha = 0.8) = 2.34$ ,  $A(\alpha = 1.1) = 1.86$ , and  $A(\alpha = 2) = 1.73$ . On the other hand, it is natural that the amplitude increases and width decreases with the growth of propagation constant  $b$ , as shown in Fig. 1(b), in agreement with the above-mentioned scaling relations. In the latter figure, the amplitudes of the fundamental soliton are  $A(b = 1) = 1.73$  and  $A(b = 2) = 2.36$ .

Next, we present the characteristics of families of fundamental solitons. First, in Fig. 2(a) we display the relation between the soliton's power  $P$ , calculated as per Eq. (6), and LI  $\alpha$ , for a fixed value of the propagation constant. It is seen that the dependence  $P(\alpha)$  is a nearly linear one. In fact, this dependence may be approximately explained by Eq. (9), as shown by the fitting line in Fig. 2(a).

The stability is determined by the dependence of the maximum real part of eigenvalues,  $\lambda_{Rm}$ , obtained from the numerical solution of Eq. (II), on  $\alpha$ , as shown in Fig.

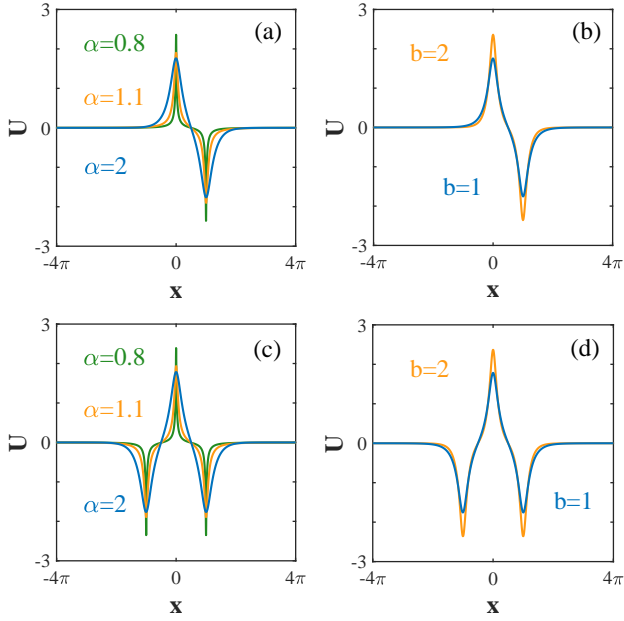


FIG. 4. Typical profiles of dipole bound states: (a) with different values of  $\alpha$  at  $b = 1$ ; (b) with different values of  $b$  at  $\alpha = 1.8$ . Profiles of tripoles: (c) with different values of  $\alpha$  at  $b = 1$ ; (d) with different values of  $b$  at  $\alpha = 1.8$ .

2(b), which identifies the respective stability region

$$\alpha > \alpha_{\text{crit}}^{(\text{fund})} \approx 1.45, \quad (10)$$

as defined by condition  $\lambda_{\text{Rm}} = 0$ . As mentioned above, the plots in Figs. 2(a) and (b) can be extended towards  $\alpha < 1$ , but in that area the fundamental solitons are definitely unstable, as suggested by Fig. 2(b).

It is well known that a necessary (but, generally, not sufficient) stability condition for bright solitons is provided by the Vakhitov-Kolokolov (VK) criterion, which is formulated in terms of the dependence of the integral power on the propagation constant:  $dP/db > 0$  [3, 78]. The relation  $P(b)$  is displayed in Fig. 2(c), which clearly complies with the VK criterion at all values of  $b$ . The  $P(b)$  dependences can be also explained in a quasi-analytical form, making use of scaling relation (9), as shown by means of fitting line in Fig. 2(c). In particular, for the value of  $\alpha = 1.5$  adopted in Fig. 2(c) Eq. (9) yields  $P \sim b^{1/3}$ .

The stability analysis is continued by data displayed in Fig. 2(d), which displays numerically exact results for the maximum instability growth rate,  $\lambda_{\text{Rm}}(b)$ , in the same interval of  $b$  that is shown in Fig. 2(c). It is seen that the stability actually takes place in a part of the interval,

$$0 \leq b < b_{\text{max}}^{(\text{fund})} \approx 2, \quad (11)$$

and unstable at  $b > b_{\text{max}}^{(\text{fund})}$ . The instability of the narrow solitons corresponding to large  $b$  may be explained by the

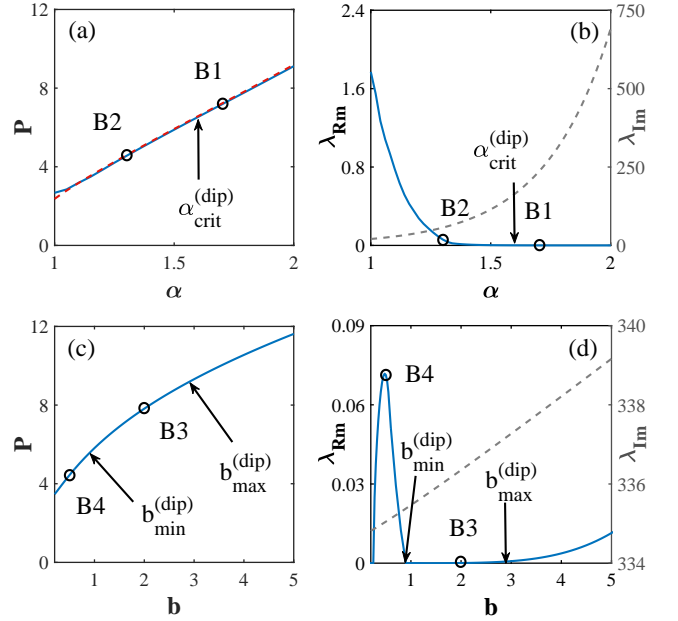


FIG. 5. Dipole bound states. Integral power  $P$  (a) and the maximum real part of perturbation eigenvalues  $\lambda_{\text{Rm}}$  (b) versus  $\alpha$  at a fixed propagation constant,  $b = 2$ . Power  $P$  (c) and  $\lambda_{\text{Rm}}$  (d) versus  $b$  for at fixed LI,  $\alpha = 1.8$ . Similar to Fig. 2, arrows in panels (b) and (d) indicate boundaries of the respective stability regions, the instability being very weak to the left of the boundary in (b). A cardinal difference from the fundamental solitons (cf. Fig. 2(d)) is that the stability region for the dipoles in panel (d) is bounded on the side of small  $b$ . The red dashed line in (a) displays the data for the fundamental solitons from Fig. 2(a), with the same propagation constant,  $b = 2$ , multiplied by 2. Panels (b) and (d) also include the imaginary part  $\lambda_{\text{Im}}$  corresponding to  $\lambda_{\text{Rm}}$  (gray dashed lines). Perturbed propagation of the dipoles marked by B1–B4 are displayed in Figs. 7(a–d), respectively.

fact that the effectively nonlocal fractional-diffraction operator cannot provide the stability of very narrow modes, unlike the usual local operator corresponding to  $\alpha = 2$ .

Predictions for the stability produced by the computation of  $\lambda_{\text{Rm}}$  have been verified by direct simulations of the evolution of the fundamental solitons performed in the framework of the full nonlinear equation (1), as shown in Fig. 3. In the simulations, random initial perturbations at the 1% amplitude level were added to the input. In Fig. 3 the left and right column display the stable and unstable propagation, respectively. In the former case, the solitons with  $\lambda_{\text{Rm}} = 0$  demonstrate completely stable evolution up to  $z = 1000$ , which corresponds, with  $A \simeq 2$  (see Fig. 1) to  $\sim 5000$  characteristic nonlinearity lengths,  $z_{\text{nonlin}} \sim A^{-2}$ . On the other hand, unstable solitons with  $\lambda_{\text{Rm}} > 0$  oscillate irregularly in Fig. 3(b) or very slowly decay through the emission of small-amplitude “radiation” in Fig. 3(d). In fact, even the unstable solitons may be categorized as objects that will seem sufficiently robust ones in the experiment, as the instability devel-

opment does not destroy them. Additional simulations demonstrate that the instability, if any, keeps the same mild character at other values of the parameters.

To conclude this subsection, it is relevant to mention that the simplified model, without the quintic term and a constant coefficient in front of the cubic one, provide similar results for the shape and stability of the fundamental solitons. However, such a model is not able to produce dipole and tripole modes presented below.

### B. Dipoles and triplets

As mentioned above, the nonlinear lattice offers the possibility to create multipole bound states. Typical profiles of dipole and tripole complexes, with opposite signs of adjacent fundamental solitons that build the dipoles, are presented, severally, in Figs. 4(a,b) and (c,d). The dipoles are composed, roughly speaking, of two fundamental solitons placed at adjacent local minima of the potential energy,  $x = 0$  and  $\pi$  (see Eq. (4)). Dipoles of this type are usually called intersite-centered (alias densely-packed) ones, without an empty site in the middle, which would be seen in *onsite-centered* modes. They may be stable due to the balance between repulsion between the constituents with opposite signs and pinning to the underlying lattice [79]. On the other hand, lattice-based complexes built of adjacent fundamental solitons with identical signs are unstable in accordance with the general analysis [79], therefore they are not reported here. The triplets are also built as tightly-packed complexes.

According to Figs. 4(a) and (c), amplitudes and widths of both the dipole and tripole families gradually decrease and increase, respectively, with the growth of LI  $\alpha$ , similar to what is observed above for the fundamental solitons, cf. Fig. 1(a). For example, the dipole's amplitudes are  $A(\alpha = 0.8) = 2.36$ ,  $A(\alpha = 1.1) = 1.9$  and  $A(\alpha = 2) = 1.76$ . Further, it is seen in Figs. 4(b) and (d) that the amplitude and width, respectively, gradually increase and decrease with the growth of propagation constant  $b$ , also similar to properties of the fundamental solitons shown in Fig. 1(b). Accordingly, typical values of the dipole's amplitude are  $A(b = 1) = 1.75$ , and  $A(b = 2) = 2.36$ .

Proceeding to characteristics of the family of dipole states, the respective relation between the integral power  $P$ , as defined by Eq. (6), and LI  $\alpha$  is displayed in Fig. 5(a), which shows a linear growth of  $P$  with  $\alpha$ . In fact, this  $P(\alpha)$  curve is nearly identical to its counterpart for the fundamental solitons, displayed for the same fixed value of the propagation constant,  $b = 2$ , in Fig. 2(a), multiplied by 2. Similar to the case of the fundamental solitons (cf. Fig. 2(a)), this dependence can be explained, although with poorer accuracy, by scaling relation (9), as shown by the fitting curve in 5(a). Next, the maximum real part of the perturbation eigenvalues for the dipoles,  $\lambda_{Rm}$ , produced by the numerical solution of Eq. (11), is displayed, as a function of  $\alpha$  in Fig. 5(b),

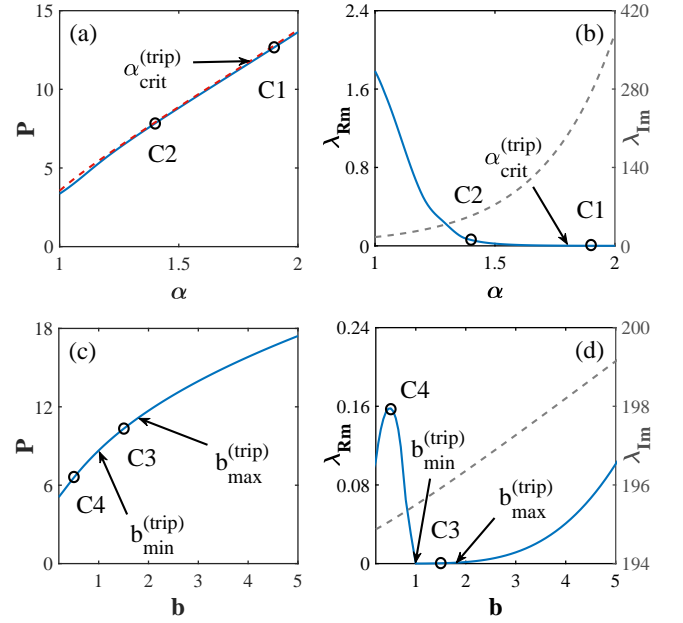


FIG. 6. Characteristics of the tripole complexes. Integral power  $P$  (a) and the maximum real part of perturbation eigenvalues  $\lambda_{Rm}$  (b) versus  $\alpha$  at a fixed propagation constant,  $b = 2$ . Power  $P$  (c) and  $\lambda_{Rm}$  (d) versus  $b$  at fixed LI,  $\alpha = 1.8$ . Similar to Fig. 5, arrows in (b) and (d) indicate boundaries of the respective stability regions. The red dashed line in (a) displays the data for the fundamental solitons from Fig. 2(a), with the same propagation constant,  $b = 2$ , multiplied by 3. Panels (b) and (d) also include the imaginary part  $\lambda_{Im}$  (gray dashed lines) corresponding to  $\lambda_{Rm}$ . Simulations of the perturbed propagations of the tripole states marked by C1–C4 are displayed in Figs. 8(a–d), respectively.

demonstrating the stability region

$$\alpha > \alpha_{crit}^{(dip)} \approx 1.6, \quad (12)$$

which is slightly narrower than its counterpart for the fundamental solitons given by Eq. (10).

Another characteristic of the dipole family is  $P(b)$  dependence, displayed in versus  $b$  in Fig. 5(c), which satisfies the VK criterion. Note that the  $P(b)$  dependence is still very accurately approximated by scaling relation (9), as shown by the fitting curve in the figure. The corresponding dependence of the instability growth rate,  $\lambda_{Rm}$ , on  $b$  is displayed in Fig. 5(d). This plot demonstrates a drastic difference from its counterpart for fundamental solitons in Fig. 2(d), as the stability interval for the dipoles is a *window*, bounded both from above and from below,

$$b_{min}^{(dip)} \approx 0.9 < b < b_{max}^{(dip)} \approx 2.9, \quad (13)$$

cf. Eq. (11). The instability of broad dipoles corresponding to small values of the propagation constant,  $b < b_{min}^{(dip)}$ , is explained by the fact that the strong overlap between broad constituent solitons that build the dipole



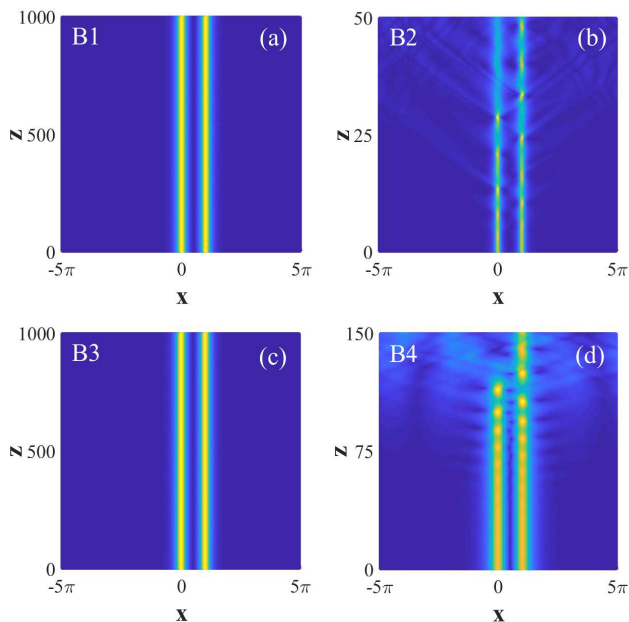


FIG. 7. The propagation of perturbed dipole solitons: (a) a stable soliton at  $\alpha = 1.7$ ,  $b = 2$ ; (b) an unstable one at  $\alpha = 1.3$ ,  $b = 2$ ; (c) a stable soliton at  $\alpha = 1.8$ ,  $b = 2$ ; (d) an unstable one at  $\alpha = 1.8$ ,  $b = 0.5$ .

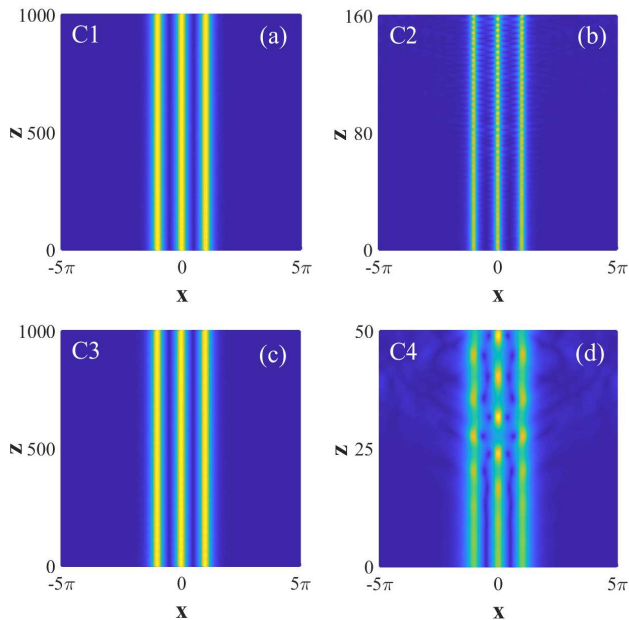


FIG. 8. The propagation of perturbed tripole solitons: (a) a stable one at  $\alpha = 1.9$ ,  $b = 2$ ; (b) an unstable soliton at  $\alpha = 1.4$ ,  $b = 2$ ; (c) a stable one at  $\alpha = 1.8$ ,  $b = 1.5$ ; (d) an unstable soliton at  $\alpha = 1.8$ ,  $b = 0.5$ .

leads to strong interaction between them, which produces a destabilizing effect.

For the tripole complexes the relation between the in-

tegral power,  $P$ , and LI  $\alpha$  is presented in Fig. 6(a). This nearly linear  $P(\alpha)$  dependence is very close to its counterpart for the fundamental solitons, displayed for the same fixed  $b = 2$ , in Fig. 2(a), multiplied by 3 (again satisfying the VK criterion), similar to the above notice that the  $P(\alpha)$  curve in Fig. 5(a) is closely approximated by its counterpart for the fundamental solitons from Fig. 2(a) multiplied by 3. Next, in Fig. 6(b) the maximum real part of eigenvalues  $\lambda_{Rm}$ , produced by the numerical solution of Eq. (II), is displayed as a function of  $\alpha$ , the respective stability region being

$$\alpha > \alpha_{\text{crit}}^{(\text{trip})} \approx 1.8, \quad (14)$$

which is narrower than its counterpart (12) for the dipoles. The same eigenvalue is plotted versus the propagation constant  $b$  in Fig. 6(d). In terms of  $b$ , the stability window is

$$b_{\text{min}}^{(\text{trip})} \approx 1 < b < b_{\text{max}}^{(\text{trip})} \approx 1.8, \quad (15)$$

which is considerably smaller than a similar one (13) for the dipoles. It is not surprising that the more complex bound states (tripoles) is more fragile than simpler ones, arranged as dipoles.

Direct simulations of the perturbed propagation of dipole states are presented in Fig. 7, in which the left and right columns refer, respectively, to the stable and unstable propagation. According to the left column, stable dipoles keep their shapes in the course of the very long propagation, up to  $z = 1000$ . On the other hand, those dipoles that are predicted to be unstable by means of the linear-stability analysis feature irregular oscillations and gradual decay through the emission of small-amplitude waves, in the right column of Fig. 7. Similarly, in Fig. 8, stable tripoles keep their shapes in the left column, while their unstable counterparts also demonstrate irregular oscillations and gradual decay.

#### IV. CONCLUSION

In this work, a one-dimensional model combining the fractional diffraction and nonlinear CQ (cubic-quintic) lattice is introduced, and families of fundamental and multipole (dipole and tripole) solitons in it are reported. The shapes and stability of these states are established by means of the systematic numerical investigation. Some results are explained with the help of the analytical approximation, which is based on the consideration of scaling properties of the underlying equation. The solitons are stable above a critical value of the LI (Lévy index),  $\alpha$ . In terms of the propagation constant,  $b$ , the fundamental solitons are stable below a critical value, while the dipole and tripole complexes are stable in intervals of  $b$  limited from above and below. The stability areas of all the states, predicted by the calculation of the perturbation eigenvalues, are corroborated by direct simulations of the perturbed evolution. In the simulations, the instability

of some states seems weak, which suggests that they may also represent relevant objects for experimental observation. Naturally, the stability regions, in terms of both  $\alpha$  and  $b$ , are widest for the fundamental solitons, and narrowest for the most complex states, *viz.*, the *tripoles*.

As an extension of the present analysis, it may be interesting to consider mobility of the solitons on top of the underlying nonlinear lattice, and collisions between moving ones. A straightforward extension may also address bound states of more than three solitons, and dynamics of multi-soliton arrays pinned to the nonlinear CQ lattice.

## DECLARATION OF COMPETING INTEREST

The authors declare that they have no known competing financial interests or personal relationships that

could have appeared to influence the work reported in this paper.

## FUNDING

National Major Instruments and Equipment Development Project of National Natural Science Foundation of China (No. 61827815); National Natural Science Foundation of China (No. 62075138); Science and Technology Project of Shenzhen (JCYJ20190808121817100, JCYJ20190808164007485); Israel Science Foundation (grant No. 1286/17).

- 
- [1] Kivshar YS, Agrawal GP. Optical solitons: from fibers to photonic crystals. San Diego: Academic; 2003.
  - [2] Kivshar YS, Luther-Davies B. Dark optical solitons: physics and applications. Phys Rep 1998;298(2-3):81-197.
  - [3] Bergé L. Wave collapse in physics: principles and applications to light and plasma waves. Phys Rep 1998;303(5-6):259-370.
  - [4] Bergé L. Soliton stability versus collapse. Phys Rev E 2000;62(3):R3071-74.
  - [5] Malomed BA, Mihalache D, Wise F, Torner L. Spatiotemporal optical solitons. J Opt B 2005;7(5):R53-R72 ; Viewpoint: On multidimensional solitons and their legacy in contemporary Atomic, Molecular and Optical physics. J Phys B 2016;49(17):170502.
  - [6] Chen Z, Segev M, Christodoulides DN. Optical spatial solitons: historical overview and recent advances. Rep Progr Phys 2012;75(8):086401.
  - [7] Malomed BA. Multidimensional solitons: Well-established results and novel findings. Eur Phys J Spec Top 2016;225(13-14):2507-32.
  - [8] Kartashov YV, Astrakharchik GE, Malomed BA, Torner L. Frontiers in multidimensional self-trapping of nonlinear fields and matter. Nature Rev Phys 2019;1(3):185-97.
  - [9] Malomed BA, Mihalache D. Nonlinear waves in optical and matter-wave media: A topical survey of recent theoretical and experimental results. Rom J Phys 2019;64(5-6):106.
  - [10] Mihalache D. Multidimensional localized structures in optical and matter-wave media: A topical survey of recent literature. Rom Rep Phys 2017;69(1):403.
  - [11] Efremidis NK, Hudock J, Christodoulides DN, Fleischer JW, Cohen O, Segev M. Two-dimensional optical lattice solitons. Phys Rev Lett 2003;91(21):213906.
  - [12] Yang J, Musslimani ZH. Fundamental and vortex solitons in a two-dimensional optical lattice. Opt Lett 2003;28(21):2094-6.
  - [13] Neshev D, Ostrovskaya E, Kivshar Y, Krolikowski W. Spatial solitons in optically induced gratings. Opt Lett 2003;28(9):710-2.
  - [14] Fleischer JW, Segev M, Efremidis NK, Christodoulides DN. Observation of two-dimensional discrete solitons in optically induced nonlinear photonic lattices. Nature 2003;422(6928):147-50.
  - [15] Kartashov YV, Egorov AA, Torner L, Christodoulides DN. Stable soliton complexes in two-dimensional photonic lattices. Opt Lett 2004;29(16):1918-20.
  - [16] Mihalache D, Mazilu D, Lederer F, Kivshar YS. Collisions between discrete surface spatiotemporal solitons in nonlinear waveguide arrays. Phys Rev A 2009;79(1):013811.
  - [17] Brazhnyi VA, Konotop VV. Theory of nonlinear matter waves in optical lattices. Mod Phys Lett B 2004;18(14):627-51.
  - [18] Morsch O, Oberthaler M. Dynamics of Bose-Einstein condensates in optical lattices. Rev Mod Phys 2006;78(1):179-215.
  - [19] Kartashov YV, Vysloukh VA, Torner L. Soliton shape and mobility control in optical lattices. Prog Opt 2009;52:63-148.
  - [20] Kartashov YV, Vysloukh VA, Torner L. Solitons in complex optical lattices. Eur Phys J Spec Top 2009;173(1):87-105.
  - [21] Yang J. Nonlinear Waves in Integrable and Nonintegrable Systems, Philadelphia: SIAM; 2010.
  - [22] Zeng L, Zeng J. Gap-type dark localized modes in a Bose-Einstein condensate with optical lattices. Adv Photonics 2019;1(4):046004.
  - [23] Zhang Y, Wu B. Composition Relation between Gap Solitons and Bloch Waves in Nonlinear Periodic Systems. Phys Rev Lett 2009;102(9):093905.
  - [24] Rose P, Richter T, Terhalle B, Imbrock J, Kaiser F, Denz C. Discrete and dipole-mode gap solitons in higher-order nonlinear photonic lattices. Appl Phys B 2007;89(4):521-6.
  - [25] Baizakov BB, Malomed BA, Salerno M. Multidimensional solitons in periodic potentials. Europhys Lett 2003;63(5):642-8.
  - [26] Baizakov BB, Malomed BA, Salerno M. Multidimensional solitons in a low-dimensional periodic potential.

- Phys Rev A 2004;70(5):053613.
- [27] Yang J. Stability of vortex solitons in a photorefractive optical lattice. *New J Phys* 2004;6(1):47.
  - [28] Kartashov YV, Malomed BA, Torner L. Solitons in nonlinear lattices. *Rev Mod Phys* 2011;83(1):247-306.
  - [29] Kartashov YV, Vysloukh VA, Torner L. Propagation of solitons in thermal media with periodic nonlinearity. *Opt Lett* 2008;33(15):1774-6.
  - [30] Kartashov YV, Malomed BA, Vysloukh VA, Torner L. Two-dimensional solitons in nonlinear lattices. *Opt Lett* 2009;34(6):770-2.
  - [31] Abdullaev FKh, Kartashov YV, Konotop VV, Zezyulin DA. Solitons in  $\mathcal{PT}$ -symmetric nonlinear lattices. *Phys Rev A* 2011;83(4):041805(R).
  - [32] Kartashov YV, Vysloukh VA, Torner L. Soliton modes, stability, and drift in optical lattices with spatially modulated nonlinearity. *Opt Lett* 2008;33(15):1747-9.
  - [33] Sakaguchi H, Malomed BA, Solitons in combined linear and nonlinear lattice potentials. *Phys Rev A* 2010;81(1):013624.
  - [34] He Y, Zhu X, Mihalache D, Liu J, Chen Z. Lattice solitons in  $\mathcal{PT}$ -symmetric mixed linear-nonlinear optical lattices. *Phys Rev A* 2012;85(1):013831.
  - [35] Borovkova OV, Kartashov YV, Torner L, Malomed BA. Bright solitons from defocusing nonlinearities. *Phys. Rev. E* 2011;84(3):035602(R).
  - [36] Borovkova OV, Kartashov YV, Malomed BA, Torner L. Algebraic bright and vortex solitons in defocusing media. *Opt Lett* 2011;36(16):3088-90.
  - [37] Dror N, Malomed BA. Solitons and vortices in nonlinear potential wells. *J Opt* 2016;16:014003.
  - [38] Lobanov VE, Borovkova OV, Kartashov YV, Malomed BA, Torner L. Stable bright and vortex solitons in photonic crystal fibers with inhomogeneous defocusing nonlinearity. *Opt Lett* 2012;37(11):1799-801.
  - [39] Tian Q, Wu L, Zhang Y, Zhang J-F. Vortex solitons in defocusing media with spatially inhomogeneous nonlinearity. *Phys Rev E* 2012;85(5):056603.
  - [40] Wu Y, Xie Q, Zhong H, Wen L, Hai W. Algebraic bright and vortex solitons in self-defocusing media with spatially inhomogeneous nonlinearity. *Phys Rev A* 2013;87(5):055801.
  - [41] Driben R, Kartashov YV, Malomed BA, Meier T, Torner L. Three-dimensional hybrid vortex solitons. *New J Phys* 2014;16(6):063035.
  - [42] Kartashov YV, Malomed BA, Vysloukh VA, Belić MR, Torner L. Rotating vortex clusters in media with inhomogeneous defocusing nonlinearity. *Opt Lett* 2017;42(3):446-9.
  - [43] Zeng L, Zeng J. Modulated solitons, soliton and vortex clusters in purely nonlinear defocusing media. *Ann Phys* 2020;421:168284.
  - [44] Kartashov YV, Malomed BA, Shnir Y, Torner L. Twisted toroidal vortex solitons in inhomogeneous media with repulsive nonlinearity. *Phys Rev Lett* 2014;113(26):264101.
  - [45] Driben R, Kartashov YV, Malomed BA, Meier T, Torner L. Soliton gyroscopes in media with spatially growing repulsive nonlinearity. *Phys Rev Lett* 2014;112(2):020404.
  - [46] Zeng L, Zeng J, Kartashov YV, Malomed BA. Purely Kerr nonlinear model admitting flat-top solitons. *Opt Lett* 2019;44(5):1206-9.
  - [47] Zeng L, Zeng J. Gaussian-like and flat-top solitons of atoms with spatially modulated repulsive interactions. *J Opt Soc Am B* 2019;36(8):2278-84.
  - [48] Hukriede J, Runde D, Kip D. Fabrication and application of holographic Bragg gratings in lithium niobate channel waveguides. *J Phys D* 2003;36(3):1-16.
  - [49] Enomoto K, Kasa K, Kitagawa M, Takahashi Y. Optical Feshbach Resonance Using the Intercombination Transition. *Phys Rev Lett* 2008;101(20):203201.
  - [50] Bauer DM, Lettner M, Vo C, Rempe G, Dürr S. Control of a magnetic Feshbach resonance with laser light. *Nat Phys* 2009;5(5):339-42.
  - [51] Yamazaki R, Taie S, Sugawa S, Takahashi Y. Sub-micron spatial modulation of an interatomic interaction in a Bose-Einstein condensate. *Phys Rev Lett* 2010;105(5):050405.
  - [52] Laskin N. Fractional quantum mechanics and Lévy path integrals. *Phys Lett A* 2000;268(4-6):298-305.
  - [53] Laskin N. Fractional quantum mechanics. *Phys Rev E* 2000;62(3):3135-45.
  - [54] Laskin N. Fractional Schrödinger equation. *Phys Rev E* 2002;66(5):056108.
  - [55] Laskin N. Fractional quantum mechanics. Singapore: World Scientific; 2018.
  - [56] Stickler BA. Potential condensed-matter realization of space-fractional quantum mechanics: The one-dimensional Lévy crystal. *Phys Rev E* 2013;88(1):012120.
  - [57] Pinsker F, Bao W, Zhang Y, Ohadi H, Dreismann A, Baumberg JJ. Fractional quantum mechanics in polariton condensates with velocity-dependent mass. *Phys Rev B* 2015;92(19):195310.
  - [58] Longhi S. Fractional Schrödinger equation in optics. *Opt Lett* 2015;40(6):1117-20.
  - [59] Zeng L, Zeng J. One-dimensional solitons in fractional Schrödinger equation with a spatially periodic modulated nonlinearity: nonlinear lattice. *Opt Lett* 2019;44(11):2661-4.
  - [60] Li P, Li J, Han B, Ma H, Mihalache D.  $\mathcal{PT}$ -symmetric optical modes and spontaneous symmetry breaking in the space-fractional Schrödinger equation. *Rom Rep Phys* 2019;71(2):106.
  - [61] Shi J, Zeng J. 1D Solitons in Saturable Nonlinear Media with Space Fractional Derivatives. *Ann Phys (Berlin)* 2020;532(1):1900385.
  - [62] Li P, Dai C. Double Loops and Pitchfork Symmetry Breaking Bifurcations of Optical Solitons in Nonlinear Fractional Schrödinger Equation with Competing Cubic-Quintic Nonlinearities, *Ann Phys (Berlin)* 2020;532(8):2000048.
  - [63] Zhong WP, Belić MR, Malomed BA, Zhang Y, Huang T. Spatiotemporal accessible solitons in fractional dimensions. *Phys Rev E* 2016;94(1):012216.
  - [64] Zhong WP, Belić MR, Zhang Y. Accessible solitons of fractional dimension. *Ann Phys* 2016;368:110-6.
  - [65] Xie J, Zhu X, He Y. Vector solitons in nonlinear fractional Schrödinger equations with parity-time-symmetric optical lattices. *Nonlinear Dyn* 2019;97(2):1287-94.
  - [66] Zeng L, Zeng J. One-dimensional gap solitons in quintic and cubic-quintic fractional nonlinear Schrödinger equations with a periodically modulated linear potential. *Nonlinear Dyn* 2019;98(2):985-95.
  - [67] Dong L, Huang C, Qi W. Nonlocal solitons in fractional dimensions. *Opt Lett* 2019;44(20):4917-20.
  - [68] Li P, Malomed BA, Mihalache D. Vortex solitons in fractional nonlinear Schrödinger equation with the cubic-quintic nonlinearity. *Chaos Solitons Fract* 2020;137:109783.



- [69] Qiu Y, Malomed BA, Mihalache D, Zhu X, Peng X, He Y. Stabilization of single- and multi-peak solitons in the fractional nonlinear Schrödinger equation with a trapping potential. *Chaos Solitons Fract* 2020;140:110222.
- [70] Zeng L, Zeng J. Preventing critical collapse of higher-order solitons by tailoring unconventional optical diffraction and nonlinearities. *Commun Phys* 2020;3(1):26.
- [71] Li P, Malomed BA, Mihalache D. Metastable soliton necklaces supported by fractional diffraction and competing nonlinearities. *Opt Express* 2020;28(23):34472-88.
- [72] Li P, Malomed BA, Mihalache D. Symmetry breaking of spatial Kerr solitons in fractional dimension. *Chaos Solitons Fract* 2020;132:109602.
- [73] Chen J, Zeng J. Spontaneous symmetry breaking in purely nonlinear fractional systems. *Chaos* 2020;30(6):063131.
- [74] Zeng L, Zeng J. Fractional quantum couplers. *Chaos Solitons Fract* 2020;140:110271.
- [75] Qiu Y, Malomed BA, Mihalache D, Zhu X, Zhang L, He Y. Soliton dynamics in a fractional complex Ginzburg-Landau model. *Chaos Solitons Fract* 2020;131:109471.
- [76] Zhang Y, Liu X, Belić MR, Zhong W, Zhang Y, Xiao M. Propagation dynamics of a light beam in a fractional Schrödinger equation. *Phys Rev Lett* 2015;115(18):180403.
- [77] Yang J, Lakoba TI. Universally-convergent squared-operator iteration methods for solitary waves in general nonlinear wave equations. *Stud Appl Math* 2007;118(2):153-97.
- [78] Vakhitov NG, Kolokolov AA. Stationary solutions of the wave equation in a medium with nonlinearity saturation. *Radiophys Quantum Electron* 1973;16(7):783-9.
- [79] Kapitula T, Kevrekidis PG, Malomed BA. Stability of multiple pulses in discrete systems. *Phys Rev E* 2001;63(3):036604.